Chinese Chemical Letters 37 (2026) 111607

Contents lists available at ScienceDirect

Chinese Chemical Letters

journal homepage: www.elsevier.com/locate/cclet

Self-propelled biomotors co-deliver doxorubicin liposomes and aPD-1 antibody to fight breast cancer

Jia Wang[a,1], Yunxiu Fan[b,1], Shilin Xu[a,1], Zhouxue Wu[a], Tian Hu[a], Yun Lu[a], Yue Li[c], Kang Xiong[a], Hongjun Deng[a], Jingrong Huang[a], Bo Yang[b,*], Shaozhi Fu[a,d,*]

[a] Department of Oncology, the Affiliated Hospital of Southwest Medical University, Luzhou 646000, China
[b] Cancer center, Chongqing University Three Gorges Hospital, Chongqing 404000, China
[c] Medicine and Health Klinikum Rechts der Isar, Technical University of Munich, München 81675, Germany
[d] Nuclear Medicine and Molecular Imaging Key Laboratory of Sichuan Province, Luzhou 646000, China

ARTICLE INFO

Article history:
Received 29 April 2025
Revised 15 July 2025
Accepted 18 July 2025
Available online 18 July 2025

Keywords:
Anaerobic bacteria
Liposome
Doxorubicin
Anti-PD-1 antibody
Chemo-immunotherapy
Breast cancer

ABSTRACT

Although the combination of chemotherapy and immunotherapy can improve the treatment of breast cancer, traditional drugs are highly toxic because they do not specifically target tumors. In this study, we developed a self-driving bacteria/nanoparticle biohybrid called Bif@PDA-aPD1/DOX-Lip by attaching polydopamine (PDA) coated doxorubicin (DOX) liposomes and the immune checkpoint inhibitor anti-programmed cell death protein 1 antibody (aPD-1) to *Bifidobacterium infantis* (*B. infantis*, Bif). Using the homing abilities of bacteria, Bif@PDA-aPD1/DOX-Lip could actively accumulate in tumor tissue, releasing DOX and aPD-1 in the acidic environment to have a synergistic anti-tumor effect. Results show that the concentration of DOX in tumors of the Bif@PDA-aPD1/DOX-Lip group was 6.31 times higher than in the free DOX group. The combination of DOX and aPD-1 not only killed tumor cells but also promoted immune normalization by maturing dendritic cells (DCs), increasing M1 macrophage ratio, and enhancing infiltration of $CD8^+$ and $CD4^+$ T cells in tumors and spleen. Therefore, Bif@PDA-aPD1/DOX-Lip therapy significantly inhibited tumor growth and increased the average survival time of mice to over 80 days. The Bif@PDA-aPD1/DOX-Lip biomotors offer a highly effective method for enhancing chemo-immunotherapy in solid tumors.

© 2025 Published by Elsevier B.V. on behalf of Chinese Chemical Society and Institute of Materia Medica, Chinese Academy of Medical Sciences.

Breast cancer is the most common diagnosed cancer in women worldwide [1–3]. Chemotherapy is the main treatment option for breast cancer patients who are not candidates for surgery [2–6]. However, traditional chemotherapeutic agents often have limited effectiveness and high toxicity [7]. Doxorubicin (DOX) is commonly used for treating solid tumors in clinical practice [8], but its low specificity and high risk of cardiotoxicity restrict its use [9–11]. Advances in material science and nanotechnology have led to the development of nanomedicines, which aim to improve drug distribution in tumors while reducing systemic toxicity [12–14]. While doxorubicin liposomes, the first Food and Drug Administration (FDA)-approved nanomedicine in 1995, have shown promise in reducing cardiac toxicity, they have not significantly improved clinical outcomes. In addition, using a single treatment alone is often not enough to effectively suppress tumors [15,16].

In recent years, immune checkpoint blockade (ICB) therapy has been widely used in clinical treatment [17–20]. However, only a minority of patients benefit from single treatment due to the immune suppressive tumor microenvironment (TME) and immune-related adverse events [21–23]. To improve the limited efficacy of single treatment, clinical guidelines recommend the combination therapy of chemotherapy and immunotherapy [24]. Several studies have demonstrated that the combination therapy of DOX with ICB therapy has a synergistic anti-tumor effect [25,26]. The synergistic mechanism involves enhance anti-tumor immunity by increasing the release of tumor associated antigens and activating dendritic cells (DCs) and T cells [27]. When combined with ICB therapy, this helps to block tumor cell immune escape, and achieve an enhanced anti-tumor therapeutic effect. Therefore, the combination therapy of chemotherapy and immunotherapy is considered an ideal strategy for fighting triple-negative breast cancer (TNBC).

However, the presence of multiple biological barriers within solid tumors significantly limits the penetration efficiency of nanomedicines, ultimately leading to suboptimal therapeutic outcomes [28–30]. Additionally, anti-programmed cell death protein

* Corresponding authors.
E-mail addresses: silenceyb1988@163.com (B. Yang), shaozhifu513@163.com (S. Fu).
[1] These authors contributed equally to this work.

https://doi.org/10.1016/j.cclet.2025.111607
1001-8417/© 2025 Published by Elsevier B.V. on behalf of Chinese Chemical Society and Institute of Materia Medica, Chinese Academy of Medical Sciences.

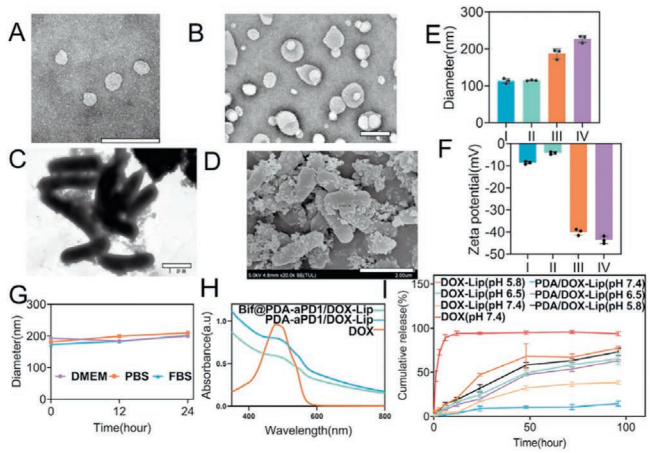


Fig. 1. *In vitro* characterization of DOX formulations. TEM images of (A) blank liposomes (Lip) (scale bar: 200 nm). (B) PDA-aPD1/DOX-Lip nanoparticles (scale bar: 100 nm), and (C) Bif@PDA-aPD1/DOX-Lip biohybrids (scale bar: 1 μm). (D) SEM image of the Bif@PDA-aPD1/DOX-Lip biohybrids (scale bar: 1 μm). (E) Average particle size and (F) zeta-potential of Lip (I), DOX-Lip (II), PDA/DOX-Lip (III), and PDA-aPD1/DOX-Lip (IV) ($n = 3$). (G) Changes of the particle size of the PDA-aPD1/DOX-Lip nanoparticles in DMEM, phosphate buffered saline (PBS), and fetal bovine serum (FBS) at 37 °C. (H) UV–vis absorption spectra of free DOX, PDA-aPD1/DOX-Lip NPs, and the Bif@PDA-aPD1/DOX-Lip solution. (I) *In vitro* release profiles of free DOX, DOX-Lip, and PDA/DOX-Lip in PBS at pH 5.8, 6.5, and 7.4 ($n = 3$). Data are presented as mean ± SD.

1 antibodies (aPD-1) often exhibit immune-related adverse events due to their non-specific distribution [5,31]. These challenges have prompted researchers to develop novel drug delivery systems that can simultaneously deliver chemoimmunotherapeutic drugs to tumor tissues. Since solid tumors are typically characterized by hypoxia, we can utilize the inherent characteristic of anaerobic microorganisms that tend towards hypoxic environments to deliver drugs into the tumors [32]. In our previous studies, *Bifidobacterium infantis* (*B. infantis*, Bif) has been used to deliver DOX-loaded metal-organic framework (MOF) nanoparticles, DOX/indocyanine green (ICG) nanoparticles, and DOX albumin nanoparticles to the hypoxic regions of tumors to enhance treatment efficacy [7,10,32]. However, a bacteria-mediated chemo-immunotherapy dual-drug co-delivery system has not yet been developed.

In this study, we used anaerobic *B. infantis* as delivery vehicles because it is a probiotic with good biocompatibility *in vivo*, as demonstrated in previous studies [10,32]. First, we loaded DOX into liposomes and then coated them with a thin layer of polydopamine (PDA). Additionally, aPD-1 was conjugated to the surface of PDA using a Michael addition reaction. Subsequently, we created self-driving biomotor Bif@PDA-aPD1/DOX-Lip by utilizing the adhesive properties of the catechol molecules in PDA to link PDA-aPD1/DOX-Lip nanoparticles onto bacterial surfaces [33].

In this study, biohybrid Bif@PDA-aPD1/DOX-Lip was synthesized according to the schematic diagram shown in Fig. S1 (Supporting information). Transmission electron microscope (TEM) images show that the blank liposome (Fig. 1A) and the PDA-aPD1/DOX-Lip nanoparticles (Fig. 1B) were spherical, demonstrating that the loading of DOX and aPD-1 did not alter their morphology. Images of TEM (Fig. 1C) and scanning electron microscope (SEM) (Fig. 1D) of the Bif@PDA-aPD1/DOX-Lip biohybrids suggest that the PDA-aPD1/DOX-Lip nanoparticles can tightly adhere to the surface of bacteria. The average particle sizes (Fig. 1E) of the blank liposome (Lip), DOX-Lip, PDA/DOX-Lip, and PDA-aPD1/DOX-Lip were measured to be 113.28 ± 6.78, 114.72 ± 1.37, 186.83 ± 13.8, and 227.06 ± 9.78 nm, respectively. The zeta potentials (Fig. 1F) were measured as -8.56 ± 0.66, -4.21 ± 0.63, -39.97 ± 1.46, and -43.57 ± 1.66 mV, respectively. Ultraviolet-visible (UV–vis) absorption spectroscopy (Fig. 1H) demonstrates that the Bif@PDA-aPD1/DOX-Lip and PDA-aPD1/DOX-Lip solutions had the same absorbance peak at 485 nm, indicating successful DOX loading and biohybrids construction. Agarose gel electrophoresis indicates that the Bif@PDA-aPD1/DOX-Lip biohybrids showed a protein band at 50 kDa, similar to the aPD-1 band (Fig. S2 in Supporting information), confirming successful conjugation of the aPD-1 onto the biohybrids. The encapsulation efficiency and drug loading efficiency of DOX in DOX-Lip were calculated at 92.6 % and 6.9 %, respectively.

The *in vitro* stability analysis shows that there was no significant change in the particle size of liposomes at 4 °C within 6 days (Fig. S3A in Supporting information). The good stability of the PDA-aPD1/DOX-Lip nanoparticles was also confirmed in various media at 4 °C (Fig. S3B in Supporting information), 25 °C (Fig. S3C in Supporting information), and 37 °C (Fig. 1G). As depicted in Fig. 1I, the cumulative drug release rates of DOX from DOX-Lip (16.8 % ± 0.57 %) and PDA/DOX-Lip (8.86 % ± 2.78 %) were significantly lower than that of free DOX (94.31 % ± 1.27 %) within 24 h. Notably, the release rate obviously increased in acidic media (pH 6.5 and 5.8). The results show that the DOX-based nanomedicines (DOX-Lip and PDA/DOX-Lip) exhibited a pH-responsive release pattern. The PDA coating significantly slowed down the release of DOX, while gradually disintegrating in acidic environments and releasing drugs.

4T1 cells and AML-12 cells exhibited high cell viability being exposed to blank liposomes at high concentration of 1000 μg/mL, suggesting that the blank liposomes, which did not show significant cytotoxicity, could be considered reliable for use as a drug carrier (Figs. S4A and S5 in Supporting information). At pH 7.4 (Fig. S4B in Supporting information) and pH 6.5 (Fig. S4C in Supporting information), all formulations of DOX (free DOX, DOX-Lip, PDA/DOX-Lip, and Bif@PDA/DOX-Lip) displayed dose-dependent cytotoxicity. Free DOX had higher cytotoxicity than the nanomedicine, which was attributed to the sustained-release effect of nanoparticles. In comparison to the cytotoxicity at pH 7.4, PDA/DOX-Lip exhibited increased cytotoxicity at pH 6.5 due to the ability of the PDA coating to degrade and release DOX in an acidic environment. Similar results were also observed in A549 cells treated with Bif@PDA/DOX-Lip (Fig. S6 in Supporting information), indicating that the development of biohybrids did not impact the cytotoxicity of DOX.

The cytotoxicity of various drug formulations on 4T1 (Fig. S4F in Supporting information) and A549 (Fig. S7 in Supporting information) cells was further evaluated using live/dead cell staining at pH 6.5. No dead cells (red fluorescence) were observed in the control group, while strong fluorescence was evident in cells treated with free DOX. Bif@PDA/DOX-Lip showed a trend similar to PDA/DOX-Lip, suggesting that attaching PDA/DOX-Lip nanoparticles to Bif did not diminish the toxicity of DOX. Additionally, all formulations of DOX, including DOX-Lip, PDA/DOX-Lip, were found to be taken up by 4T1 cells (Figs. S4D and E in Supporting information) and A549 cells (Fig. S8 in Supporting information). Furthermore, the scratch tests reveal that all DOX formulations significantly impeded tumor cell migration compared to the control group in both 4T1 cells (Figs. S4G and S9 in Supporting information) and A549 cells (Figs. S10 and S11 in Supporting information).

As shown in Fig. S12A (Supporting information), there were no obvious inhibitory zones formed around each disc, indicating that DOX loading had no toxic effect on the growth of Bif. Moreover, the binding of PDA-aPD1/DOX-Lip NPs to Bif did not affect the bacterial growth, as demonstrated by incubating Bif@PDA-aPD1/DOX-Lip biohybrids under anaerobic condition for 48 h (Fig. S12B in Supporting information). Transwell chambers were used to simulate hypoxic and normoxic environments *in vitro* (Fig. S12C in Supporting information). After 2 h of cultivation, the number of Bif in the hypoxic chamber was significantly higher than in the normoxic chamber (Fig. S12D in Supporting information), indicating that the

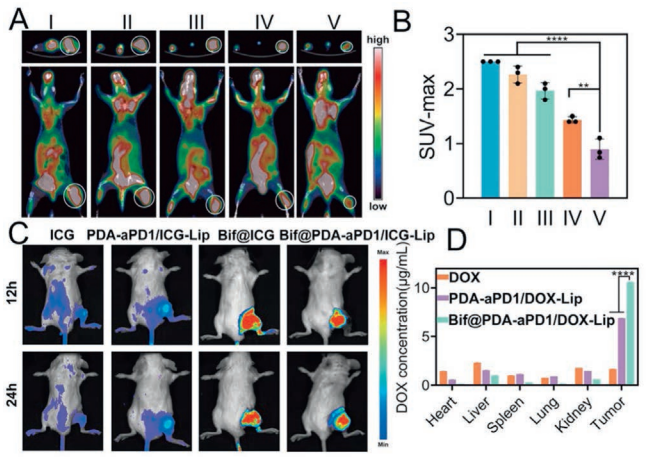


Fig. 2. *In vivo* evaluation of early treatment response, targeting ability, and drug distribution in 4T1 tumor-bearing mice. (A) Representative images of 18F-FDG PET/CT on day 12 of treatment, the upper layer: the cross-sectional images, the lower layer: the coronal images (I: control, II: Bif, III: DOX+aPD-1, IV: PDA-aPD1/DOX-Lip, V: Bif@PDA-aPD1/DOX-Lip). White circles indicate tumor sites. (B) SUV-Max of each group ($n = 3$). (C) Fluorescence images of 4T1 tumor-bearing mice after intravenous injection of free ICG, PDA-aPD1/ICG-Lip, Bif@ICG, and Bif@PDA-aPD1/ICG-Lip. (D) DOX concentrations in major organs and tumors ($n = 3$). Data are presented as mean ± SD. $^{**}P < 0.01$, $^{****}P < 0.0001$.

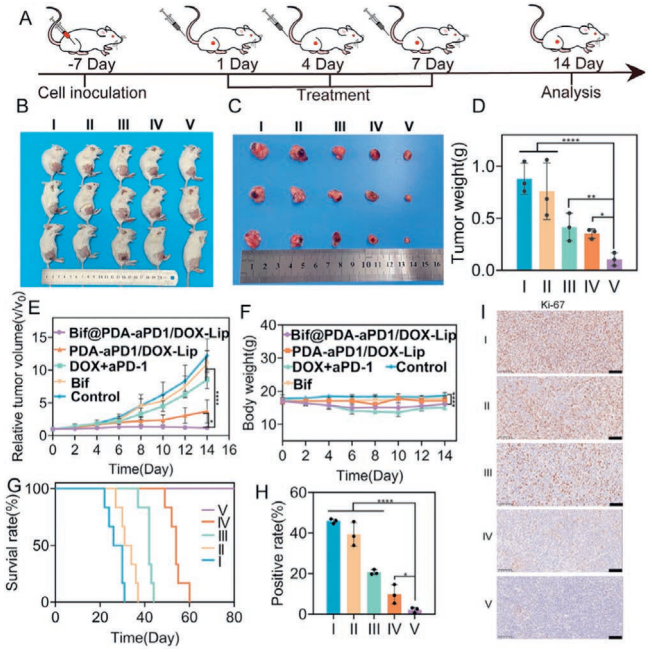


Fig. 3. *In vivo* evaluation of antitumor efficacy. (A) A schematic diagram of the treatment procedure. (B) Representative photographs of 4T1 tumor-bearing mice were taken on day 14 after treatments ($n = 3$). (C) Representative photographs of isolated tumors ($n = 3$). (D) Weight of tumors ($n = 3$). (E) Relative change in tumor volume (v/v_0) ($n = 6$). (F) Body weight fluctuations during treatment ($n = 6$). (G) Survival curves of mice after treatments ($n = 6$). (H) The ratios of Ki-67 positive tumor cells ($n = 3$). (I) Immunohistochemical staining of Ki-67 (I: control, II: Bif, III: DOX+aPD-1, IV: PDA-aPD1/DOX-Lip, V: Bif@PDA-aPD1/DOX-Lip). Scale bar: 100 μm. Data are presented as mean ± SD. $^{*}P < 0.05$, $^{**}P < 0.01$, $^{****}P < 0.0001$.

Bif@PDA-aPD1/DOX-Lip biohybrids still retained the same targeting ability as Bif to the hypoxic environment.

The targeting ability of the Bif@PDA-aPD1/DOX-Lip biohybrids to tumor tissue was also investigated using 4T1 tumor-bearing mice. Animal experimental procedures were approved by the Ethics and Scientific Committee of the Animal Care and Treatment Committee of Southwest Medical University. The results show that Bif mainly distributed in tumors, liver, and kidneys, with the number of bacteria in tumors significantly higher than in other organs (Figs. S12E and S13 in Supporting information). After 7 days of injection, the number of bacteria in tumor tissue remained high. These results indicate that the Bif@PDA-aPD1/DOX-Lip biohybrids retained the targeting ability of Bif and can colonize in hypoxic tumor tissues.

The 18-FDG PET/CT images are shown in Fig. 2A, indicating that the tumor tissues of mice in the Bif@PDA-aPD1/DOX-Lip group had the lowest FDG uptake in both the transverse and longitudinal directions. Additionally, both SUV-Max and SUV-Mean in this group were the lowest among all groups, suggesting that glucose metabolism of tumor cells was significantly inhibited (Fig. 2B and Fig. S14 in Supporting information). Furthermore, treatment with Bif@PDA-aPD1/DOX-Lip significantly increased the percentage of TUNEL-positive apoptotic cells in the tumor (Fig. S15 in Supporting information), enhancing the antitumor efficacy. ICG-labelled drugs were intravenously injected into mice to verify their targeting ability *in vivo*. As shown in Fig. 2C, Bif-mediated drugs (Bif@ICG and Bif@PDA-aPD1/ICG-Lip) could actively aggregate at the tumor site and exhibited stronger fluorescence than free ICG. Strong fluorescence can be observed in the mice of both groups twenty-four hours later. *Ex-vivo* tissue fluorescence further confirms that bacteria-mediated drugs had a higher drug distribution in tumor tissues (Fig. S16 in Supporting information), indicating excellent targeting ability of both Bif and Bif@PDA-aPD1/DOX-Lip towards hypoxic tumors. The distribution of DOX in tumors and organs was detected and illustrated in Fig. 2D. The Bif@PDA-aPD1/DOX-Lip group showed the highest concentration of DOX compared to the other groups. Furthermore, the concentration of DOX in the liver and kidneys of the mice was lower in this group than in the other groups. The concentration of DOX in the tumor tissue of the hybrid drug group was 6.31 times higher than that of the free DOX group and 1.4 times higher than that of the PDA-aPD1/ICG-Lip group. This suggests that the biohybrids can transport more DOX to the tumor site and enhance the therapeutic effect due to the PDA coating, which will break in the acidic TME and release the therapeutic drugs [34].

According to the treatment plan shown in Fig. 3A, mice were administered different drugs. Compared with other treatment groups, the tumor volume and tumor weight of mice in the Bif@PDA-aPD1/DOX-Lip group were the smallest (Figs. 3B–E). Meanwhile, the survival of mice in this group was significantly prolonged, as all mice survived for over 80 days (Fig. 3G). Fig. 3F shows the change in body weight of mice during the treatment process. Significant fluctuation was observed in the DOX+aPD-1 group, indicating that the free drugs had stronger toxic side effects on mice. Treatment with Bif@PDA-aPD1/DOX-Lip greatly decreased systemic toxicity. Additionally, as shown in Fig. 3I, the results of Ki-67 staining indicate that Bif@PDA-aPD1/DOX-Lip significantly inhibited tumor cell proliferation. The percentage of Ki-67 positive cells (2.13 % ± 1.25 %) was the lowest among all groups ($P < 0.0001$, Fig. 3H).

To evaluate anti-tumor immune responses induced by the Bif@PDA-aPD1/DOX-Lip treatment, the induction of cytotoxic T lymphocytes in the tumor and spleen was evaluated. As shown in Fig. 4A, except for the control and Bif group, immunofluorescence was observed in the other three groups, indicating that the use of aPD-1 had a stimulating effect on activating anti-tumor immunity. Furthermore, the Bif@PDA-aPD1/DOX-Lip group showed the strongest immunofluorescence, suggesting the greatest infiltration of $CD4^+$ T cells and $CD8^+$ T cells in the tumor tissues. Flow cytometry analysis results show that the percentage of $CD8^+$ tumor-infiltrating T cells in the Bif@PDA-aPD1/DOX-Lip group increased to 38.8 % compared to 7.95 % in the NS group (Fig. S17A in Supporting information). Similarly, the ratio of $CD8^+/CD4^+$ T cells also

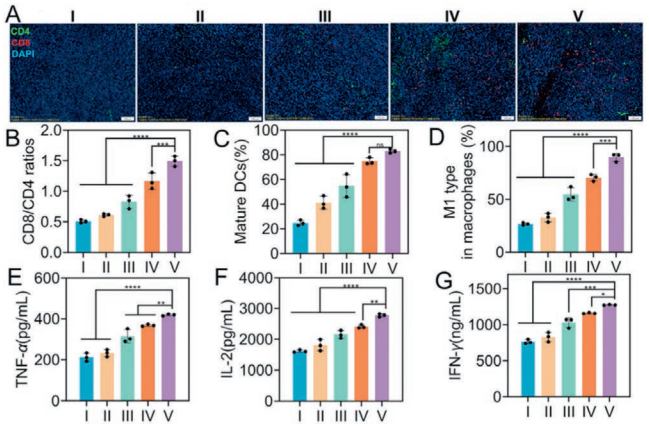


Fig. 4. *In vivo* evaluation of antitumor immune response. (A) Immunofluorescence images of CD4 and CD8 T cells in tumor. Scale bar: 100 μm. Flow cytometry analysis of CD4+ and CD8+ T cells (gated on CD45+CD3+) (B), DCs (gated on CD45+CD11C+CD11b+CD86+) (C), and M1 macrophages (gated on CD45+F4/80+CD11b+CD86+) (D) in tumor. Pro-inflammatory cytokines including TNF-α (E), IL-2 (F), and IFN-γ (G) in serum ($n = 3$). Group names: I: control, II: Bif, III: DOX+aPD-1, IV: PDA-aPD1/DOX-Lip, V: Bif@PDA-aPD1/DOX-Lip. ns: no significant difference. Data are presented as mean ± SD. $^{*}P < 0.05$, $^{**}P < 0.01$, $^{***}P < 0.001$, $^{****}P < 0.0001$.

increased to 1.5 (Fig. 4B). Maturation of dendritic cells (DCs) in the tumor was detected by flow cytometry (Fig. 4C and Fig. S17B in Supporting information), indicating that Bif@PDA-aPD1/DOX-Lip had the highest percentage (82.98% ± 1.52%) of mature DCs in the tumor, while the control group had only 24.70% ± 2.28%. The ratio of M1 macrophages in the Bif@PDA-aPD1/DOX-Lip group was significantly increased to 89.38% ± 2.88%, which was 3.3 times higher than that in the control group (Fig. 4D and Fig. S17C in Supporting information). Similar results were also observed in the spleen (Figs. S18–S20 in Supporting information).

The aforementioned results show that treatment with Bif@PDA-aPD1/DOX-Lip reshaped the immunosuppressive tumor microenvironment in mice. In accordance with this, enzyme-linked immunosorbent assay (ELISA) results demonstrate that the levels of tumor necrosis factor-alpha (TNF-α) (Fig. 4E), interleukin-2 (IL-2) (Fig. 4F), and interferon-gamma (IFN-γ) (Fig. 4G) in the serum of mice in the Bif@PDA-aPD1/DOX-Lip group significantly increased, approximately 1.97, 1.67, and 1.72 times higher than those in the control group, respectively. This indicates that treatment with Bif@PDA-aPD1/DOX-Lip induced a robust anti-tumor immune response.

Double distilled water caused complete rupture of red blood cells (100% hemolysis), while no significant hemolysis was observed in normal saline and other drugs (Figs. S21A and B in Supporting information). The hemolysis rate and UV–vis absorption spectra (Figs. S21C and D in Supporting information) confirm that the Bif@PDA-aPD1/DOX-Lip hybrids had excellent blood compatibility. Furthermore, compared to the control group, the blood routine and markers of liver/kidney function of the mice in the Bif@PDA-aPD1/DOX-Lip group were maintained within the normal range (Figs. S22 and S23 in Supporting information). The images of Masson staining of the heart indicate that only the mice in the free DOX group had mild myocardial fibrosis (Fig. S24 in Supporting information). The hematoxylin and eosin (H&E) staining images of the heart, liver, spleen, lungs, and kidneys also do not display any obvious histological damage (Fig. S25 in Supporting information).

In this study, a self-driving biohybrid Bif@PDA-aPD1/DOX-Lip was designed to co-deliver the chemotherapeutic drug DOX and the immune checkpoint inhibitor aPD-1 for the combination treatment of breast cancer. Once actively accumulated in the tumor, PDA degraded in a slightly acidic TME and released DOX and aPD-1. Treatment with the Bif@PDA-aPD1/DOX-Lip biohybrids significantly enhanced the maturation of DCs, increased the ratio of M1 macrophages, and improved the infiltration of $CD8^+$ and $CD4^+$ T cells in the tumor and spleen. Therefore, the bacteria-mediated drug delivery system may have great potential for the combination treatment of solid tumors.

Declaration of competing interest

The authors declare that they have no known competing financial interests or personal relationships that could have appeared to influence the work reported in this paper.

CRediT authorship contribution statement

Jia Wang: Writing – original draft, Data curation. **Yunxiu Fan:** Writing – original draft, Resources. **Shilin Xu:** Writing – review & editing. **Zhouxue Wu:** Formal analysis. **Tian Hu:** Writing – original draft, Data curation. **Yun Lu:** Validation. **Yue Li:** Methodology. **Kang Xiong:** Data curation. **Hongjun Deng:** Data curation. **Jingrong Huang:** Validation. **Bo Yang:** Supervision, Resources. **Shaozhi Fu:** Writing – review & editing, Funding acquisition, Conceptualization.

Acknowledgments

This study is supported by the Science and Technology Strategic Cooperation Programs of Luzhou Municipal People's Government and Southwest Medical University (No. 2024LZXNYDJ017), the Project Program of the Science and Technology Department of Sichuan Province (No. 2025ZNSFSC0679), the Project Program of Chongqing Science and Technology Bureau (No. cstc2020jcyj-msxmX1037).

Supplementary materials

Supplementary material associated with this article can be found, in the online version, at doi:10.1016/j.cclet.2025.111607.

References

[1] J. Wu, D. Fan, Z. Shao, et al., Holist. Integr. Oncol. 1 (2022) 7.
[2] L. Yang, Y. Zhang, Y. Zhang, et al., ACS Nano 16 (2022) 9799–9809.
[3] R. Lappano, M. Talia, F. Cirillo, et al., J. Exp. Clin. Cancer Res. 39 (2020) 153.
[4] X. Wu, X. Chen, X. Wang, et al., Chin. Chem. Lett. 35 (2024) 108756.
[5] Z. Zhao, L. Fang, P. Xiao, et al., Adv. Mater. 34 (2022) 2205462.
[6] W. Lu, W. Liu, A. Hu, et al., Int. J. Nanomed. 18 (2023) 861–879.
[7] J. Li, J. Dai, L. Zhao, et al., Adv. Funct. Mater. 33 (2023) 2303254.
[8] J. Wang, S. Liu, X. Meng, et al., Circ. Res. 134 (2024) 550–568.
[9] M. Ozcan, Z. Guo, C.V. Ripoll, et al., Cell Metab. 35 (2024) 928–942.
[10] Y. Lu, L. Chen, Z. Wu, et al., Biomed. Pharmacother. 169 (2023) 115846.
[11] J. Li, Q. Wen, J. Dai, et al., Int. J. Biol. Macromol. 267 (2024) 131428.
[12] R. Xie, Y. Wang, F. Tong, et al., Small 19 (2023) 2300570.
[13] W. Chen, K. Shi, Y. Yu, et al., Chin. Chem. Lett. 35 (2024) 109159.
[14] M. Liu, Y. Wang, Y. Li, et al., MedComm Biomater. Appl. 4 (2025) e70012.
[15] M.T. Manzari, Y. Shamay, H. Kiguchi, et al., Nat. Rev. Mater. 6 (2021) 351–370.
[16] C. Fan, X. Wang, Y. Wang, et al., Pharmaceutics 15 (2023) 1128.
[17] Y. Wu, Z. Zhang, Y. Wei, et al., Chin. Chem. Lett. 34 (2023) 108908.
[18] M.S. Carlino, J. Larkin, G.V. Long, Lancet 398 (2021) 1002–1014.
[19] N.S. Patil, B.Y. Nabet, S. Muller, et al., Cancer Cell 40 (2022) 289–300.e4.
[20] S. Deng, J. Wang, Y. Hu, et al., J. Nanobiotechnology 22 (2024) 156.
[21] F. Zhou, X. Li, X. Xue, et al., Adv. Healthc. Mater. 12 (2023) 2202757.
[22] G. Ma, N. Kostevsek, I. Monaco, et al., J. Control. Release 332 (2021) 419–433.
[23] T. He, L. Wang, S. Gou, et al., ACS Nano 17 (2023) 9953–9971.
[24] M. Sun, W. Shi, Y. Wu, et al., Adv. Sci. 10 (2023) 2205247.
[25] Y. Yan, A.B. Kumar, H. Finnes, et al., Front. Immunol. 9 (2018) 1739.
[26] S. Yang, M.K. Shim, W.J. Kim, et al., Biomaterials 272 (2021) 120791.
[27] B. Wei, J. Pan, R. Yuan, et al., Nano Lett. 21 (2021) 4231–4240.
[28] L. Wang, Z. Cao, M. Zhang, et al., Adv. Mater. 34 (2022) 2106669.
[29] J. Zhao, H. Huang, J. Zhao, et al., Acta Pharm. Sin. B 12 (2022) 2683–2694.
[30] X. Zhang, Z. Wei, Z. Ding, et al., Chem. Eng. J. 451 (2023) 138971.
[31] Y. Wang, X. Huang, Q. Wu, et al., MedComm. Biomater. Appl. 3 (2024) e106.
[32] S. Xiao, H. Shi, Y. Zhang, et al., J. Nanobiotechnology 20 (2022) 178.
[33] H. Guo, Z. Cao, J. Li, et al., ACS Nano 17 (2023) 5059–5071.
[34] W. Zong, Y. Hu, Y. Su, et al., J. Microencapsul. 33 (2016) 257–262.